Supplementary Information

High-Yield and Chirality-Selective Isolation of Single-Walled Carbon Nanotubes Using Conjugated Polymers and Small Molecular Chaperones

D. Just[1*], A. Dzienia[1], K.Z. Milowska[2,3], A. Mielańczyk[1], D. Janas[1*]

[1] Department of Chemistry, Silesian University of Technology, B. Krzywoustego 4, 44-100, Gliwice, Poland

[2] CIC nanoGUNE, Donostia-San Sebastián 20018, Spain

[3] Ikerbasque, Basque Foundation for Science, Bilbao 48013, Spain

* Corresponding authors: dominik.just@polsl.pl, dawid.janas@polsl.pl

Table of Contents

1. Materials

The materials used in the experiments were used as provided. The purity of the reagents, manufacturer, and reagent data are described below.

1.1. Reagents for polymer synthesis:

9,9-Dioctylfluorene-2,7-bis(boronic acid pinacol ester) (Angene, cat. number: AG0034EZ, CAS: 196207-58-6, purity: 98%), 2,5-dibromotiophene (AmBeed, cat. number: A13736710g, CAS: 3141-27-3, purity: 98%), 2,5-dibromo-3-dodecylthiophene (Ambeed, cat. number: A16618 3-25g, CAS: 148256-63-7, purity: 98%), 2,5-dibromo-3- hexylthiophene (AmBeed, cat. number: A123133, CAS: 116971-11-0, purity: 98%), thiophene (Alfa Aesar, cat. number: A13941.18, CAS: 110-02-1, purity: 99%), 2,7-dibromo-9,9-dioctyl-9H-fluorene (Sigma Aldrich, cat. number: 560073-25g, CAS: 198964-46-4, purity: 96%), 6,6'-dibromo-2,2'-bipyridyl (TCL, cat. number: D3988-5G, purity: >95%), 9-(9-heptadecanyl)-9H-carbazole-2,7-diboronic acid bis(pinacol) ester (Angene, cat. number K01-3625-1-1, CAS: 958261-51-3, purity: 95%), 5,5'-dibromo-2,2'-bipyridine (Angene, cat. number AG001Q DD-1g, CAS: 15862-18-7, 98%), Aliquat 336 TG (Alfa Aesar, cat. number: A17247, CAS: 63393-96-4, purity: N/A), tetrakis (triphenylphosphine)palladium - $Pd(PPh_3)_4$, (Apollo Scientific, cat. number: OR4225, CAS: 14221-01-3, purity: >99%), toluene (Alfa Aesar, cat. number: 19376.K2, CAS: 108-88-3, spectrophotometric grade, purity: >99.7%).

1.2. Single-walled carbon nanotubes

The study was carried out using (6,5)-enriched CoMoCAT SWCNTs (Sigma Aldrich, product number: 773735, lot: MKCM5514, purity: 95%-carbon basis) and HiPco SWCNTs (NanoIntegris, lot: HP30-006) as a reference.

2. Methods

2.1. Polymer synthesis

The synthesis of poly(9,9'-dioctylfluorenyl-2,7-diyl) (PFO), poly(9,9'-dioctylfluorenyl-2,7-diyl-*alt*-2,5-tiophene) (PFO-T), poly(9,9'-dioctylfluorenyl-2,7-diyl-*alt*-2,5-(3-hexyltiophene)) (PFO-3HT), poly(9,9'-dioctylfluorenyl-2,7-diyl-*alt*-2,5-(3-dodecyltiophene)) (PFO-3DDT), poly(9-(9-heptadecyl)-carbazoly-2,7-diyl-*alt*-6,6'-(2,2'-bipirydyl)) (PCz-BPy6,6), poly(9,9'-dioctylfluorenyl-2,7-diyl-*alt*-6,6'-(2,2'-bipyridine)) (PFO-BPy6,6), and poly(9,9'-dioctylfluorenyl-2,7-diyl-*alt*-5,5'-(2,2'-bipyridine)) (PFO-BPy5,5) were carried out by the Suzuki coupling procedure presented below. The structures of the obtained polymers were confirmed using ^{1}H NMR spectroscopy, and their macromolecular parameters were determined with size exclusion chromatography (SEC). In brief, organoboron derivative PA (9,9-di-n-octylfluorene-2,7-diboronic acid bis(pinacol)ester, purity: 98%) (0.500 g, 0.763 mmol, 1 eq.) and the appropriate amount of dibromo derivative PB (9,9-dioctyl-2,7-dibromofluorene purity: 96%) (0.418 g, 0.763 mmol, 1 eq.) was added to a high-pressure glass reactor vessel. Then, to the reactor, 1 M Na_2CO_3 solution (12 mL) and toluene (12 mL) were added. Three drops of Aliquat 336 as a phase transfer catalyst (PTC) were added. The mixture was purged with Ar for 30 min, and, subsequently, Pd(PPh$_3$)$_4$ (0.022 g, 0.019 mmol, 0.025 eq.) was added. The reaction mixture was stirred vigorously at 80 °C for 3 days. The reaction mixture was cooled, diluted with 250 mL of chloroform, and washed 4 times with 150 mL of water. The organic phase was collected and dried over anhydrous $MgSO_4$, followed by filtration. The collected material was evaporated to dryness and dissolved in a sufficient volume of chloroform (until all solid particles were dissolved, in case of excessively high concentration of the polymer promoting the formation of agglomerates during precipitation, leading to materials with lower purity). The final product was precipitated from methanol. The fibrous polymer was collected by filtration and washed twice with 50 mL of freezing methanol and then twice with 50 mL of freezing acetone.

Table S1 Selection of polymers synthesized in the study.

Name	Common Descrp.	Polymer No.	PA	PA No.	PB	PB No.
Poly(9,9'-dioctylfluorenyl-2,7-diyl-*alt*-6,6'-(2,2'-bipyridine))	PFO-BPy6,6	P1	9,9-di-n-octylfluorene-2,7-diboronic acid bis(pinacol)ester	PA1	6,6'-dibromo-2,2'-bipyridine	PB1
Poly(9,9'-dioctylfluorenyl-2,7-diyl-*alt*-5,5'-(2,2'-bipyridine))	PFO-BPy5,5	P2-3	9,9-di-n-octylfluorene-2,7-diboronic acid bis(pinacol)ester	PA1	5,5'-dibromo-2,2'-bipyridine	PB2
Poly(9,9'-dioctylfluorenyl-2,7-diyl)	PFO	P4	9,9-di-n-octylfluorene-2,7-diboronic acid bis(pinacol)ester	PA1	9,9-dioctyl-2,7-dibromofluorene	PB3
Poly(9,9'-dioctylfluorenyl-2,7-diyl-*alt*-2,5-tiophene)	PFO-T	P5-P11	9,9-di-n-octylfluorene-2,7-diboronic acid bis(pinacol)ester	PA1	2,5-dibromothiophene	PB4
Poly(9,9'-dioctylfluorenyl-2,7-diyl-*alt*-2,5-(3-dodecyltiophene))	PFO-3DDT	P12	9,9-di-n-octylfluorene-2,7-diboronic acid bis(pinacol)ester	PA1	2,5-dibromo-3-dodecylthiophene	PB6
Poly(9-(9-heptadecyl)-carbazoly-2,7-diyl-*alt*-6,6'-(2,2'-bipirydyl))	PCz-BPy6,6	P13	9-(9-heptadecanyl)-9H-carbazole-2,7-diboronic acid bis(pinacol) ester	PA2	6,6'-dibromo-2,2'-bipyridine	PB7

2.2. CPE process

In a typical dispersion process, 1.5 mg of SWCNTs and 9 mg of polymer were added to a 19 mL glass vial. Then, 5 mL of toluene was added, and the mixture was homogenized via sonication for 15 min (POLSONIC, SONIC-2, 250 W) at 5 °C. More vigorous sonication with a tip sonotrode (Hielscher UP200St ultrasonic generator) was performed to disentangle SWCNTs and wrap them with conjugated polymer. After sonication, the obtained suspension was transferred to 15 mL conical tubes and centrifuged at 9,000 rpm (15,314 × g) for 3 min, promoting the precipitation of the bundled and unwrapped SWCNTs, as well as polymer aggregates. 80% of the supernatant was transferred to a fresh vial and analyzed by UV-VIS spectroscopy and PL excitation-emission mapping.

2.3 Modelling details

2.3.1. MD/MC calculations

To investigate the impact of 2,5-dibromothiophene on the wrapping of conjugated polymers around SWCNTs, we performed a series of molecular dynamics (MD) and time-stamped force-bias Monte Carlo (MC) [1,2] simulations of infinite (6,5) SWCNT interacting with PFO-BPy6,6' polymer in toluene solution with different concentrations of 2,5-dibromothiophene molecules. Due to the applied 3D periodic boundary conditions, simulation boxes contained only 2 units of SWCNT. As shown in Fig. 3a, the initial positions of PFO-BPy6,6' with 5 repeatable AB units and SWCNT in the simulation boxes were the same in all models. Simulation boxes with dimensions sufficient to avoid direct interactions between SWCNT-polymer complex images (4.56 nm, 4.56 nm, and 8.24 nm along X, Y, and Z directions) were filled with toluene (1000 molecules) and a varying number of 2,5-dibromothiophene molecules using Packmol [3].

MD/MC simulations were performed as follows:

0) All four systems (containing 0, 10, 20, and 30 2,5-dibromothiophene molecules, respectively) were pre-optimized (500 000 steps) using FIRE algorithm [4].

1) MD simulations were first carried out in an NVT ensemble employing a Berendsen thermostat [5] at 300 K. Random initial velocities of all atoms were assigned according to the Maxwell-Boltzmann distribution. The relaxation time of the thermostat was set to 100 fs, and the simulations were carried out with a time-step of 0.1 fs over a time period of 5 ps (5,000 steps). These simulations were followed by 5 ps (50,000 steps) NPT simulations at 300 K and 1 bar by employing Berendsen thermostat and barostat. The thermostat and barostat relaxation times were set to 100 fs and 500 fs, respectively. The time step was kept the same as for the previous simulations. The estimated compressibility of the system relating volume changes to pressure changes was set to 0.0001 bar^{-1}. Then, the Martyna-Tobias-Klein [6] barostat and thermostat were used for 150 ps (1,500,000 steps) NPT simulations, employing the same parameters.

2) Next, the models were optimized (20,000 steps) using LBFGS algorithm [7] and further equilibrated in microcanonical (NVE) ensembled with a time-step of 0.5 fs over a time period of 50 ps (100,000 steps) at 300 K and again optimized using FIRE (20,000 steps) and LBFGS (50,000 steps) algorithms.

3) NVE equilibration was repeated over a time period of 0.25 ns (500,000 steps), using the same parameters, and followed by 1 ns (2,000,000 steps) NPT simulations using Martyna-Tobias-

Klein barostat and thermostat with relaxation times of 10 ps and 10 ps, respectively, to maintain the temperature (300 K) and the pressure (1 bar) in the systems. These simulations were carried out with a time-step of 0.5 fs. To investigate the interactions between the polymer and SWCNT on longer timescales, MC simulations were performed subsequently. They were carried out over a time period of 2.6557 ns (2,000,000 steps) at 300 K and 1 bar. During MC simulations, the maximum atom displacement was set to 0.05 Å, the estimated compressibility of the system related to volume changes to pressure changes was set to 0.0005 bar^{-1}, and the barostat factor was set to 1000.

4) Simulation timescales of all systems were further extended by performing additional 0.9 ns NVE simulations preceded and followed by optimization steps described in step 3) and 5.31139 ns MC simulations, using the same parameters as in step 3).

MD/MC calculations were performed using a full periodic table bonded valence forcefield - a Universal Force Field (UFF) potential [8], as implemented in QuantumATK [9,10]. Energy contributions to the UFF potential were represented by simple functions based on bond lengths, bond angles, torsion angles, inversion angles, and inter-atomic distances. The electrostatic interactions were calculated using smooth-particle-mesh-Ewald (SPME) solver [11]. The cutoff used for calculating the real-space interactions was set to 7.5 Å, while the relative accuracy of SPME summation to 0.0001. Atomic partial charges on each atom were assigned using QEq charge equilibration method [12]. Dispersive interactions were included in the form of Lennard-Jones potential [13–15] with 10 Å cutoff and 2 Å smoothing length. RDF and density profiles were calculated using the data obtained during the last 5000 ps in extended MC simulations in step 4).

2.3.2 DFT calculations

The spin-polarized Density Functional Theory (DFT) [16,17] calculations of 2,5-dibromothiophene, (6,5) SWCNT and PFO-BPy6,6' polymer of different lengths (1, 3, 5 or infinite number of repeatable units - AB) were carried out in generalized gradient approximation (GGA) employing hybrid non-local exchange and correlation functional – B3LYP [18–21] and double-ζ plus polarization numerical basis (DZP) sets, as implemented in QuantumATK [10,22]. Previous studies have shown that B3LYP functional performs reasonably well in predicting the electronic structure of different nanostructures [23–26]. The DFT calculations of 1, 3, or 5 units of PFO-BPy6,6' polymers, as well as 2,5-dibromothiophene, were performed in 'molecule configuration' mode without periodic boundary conditions applied. The Brillouin

zone was sampled only in the Γ point, while the density mesh cutoff for real-space integrals was set at 300 Ry. In the case of infinite polymer and nanotube calculations carried out in 'bulk configuration' mode with 1D periodic boundary conditions applied, the sampling of the Brillouin zone was increased to $(1 \times 1 \times 3)$ and $(1 \times 1 \times 7)$ k-points in Monkhorst and Pack scheme [27], respectively. All structures were relaxed until the maximum force acting on any atom was lower than 0.004 eV/Å, the maximum stress changed by less than 0.1 GPa, the self-consistent field (SCF) cycle was iterated until the total energy changed by less than 10^{-6} Ha, and the density matrix elements by less than 10^{-6} per iteration.

3. Characterization

3.1. Nuclear Magnetic Resonance (^{1}H NMR)

Proton nuclear magnetic resonance (^{1}H NMR) spectra of the polymers (Figures S1–S3) were registered using a Varian Unity Inova spectrometer operating at 400 MHz in CDCl$_3$ as a solvent. ^{1}H-chemical shifts were measured in δ (ppm), using the chloroform-d residual peak (set at δ 7.26) as the reference. Standard experimental conditions were used.
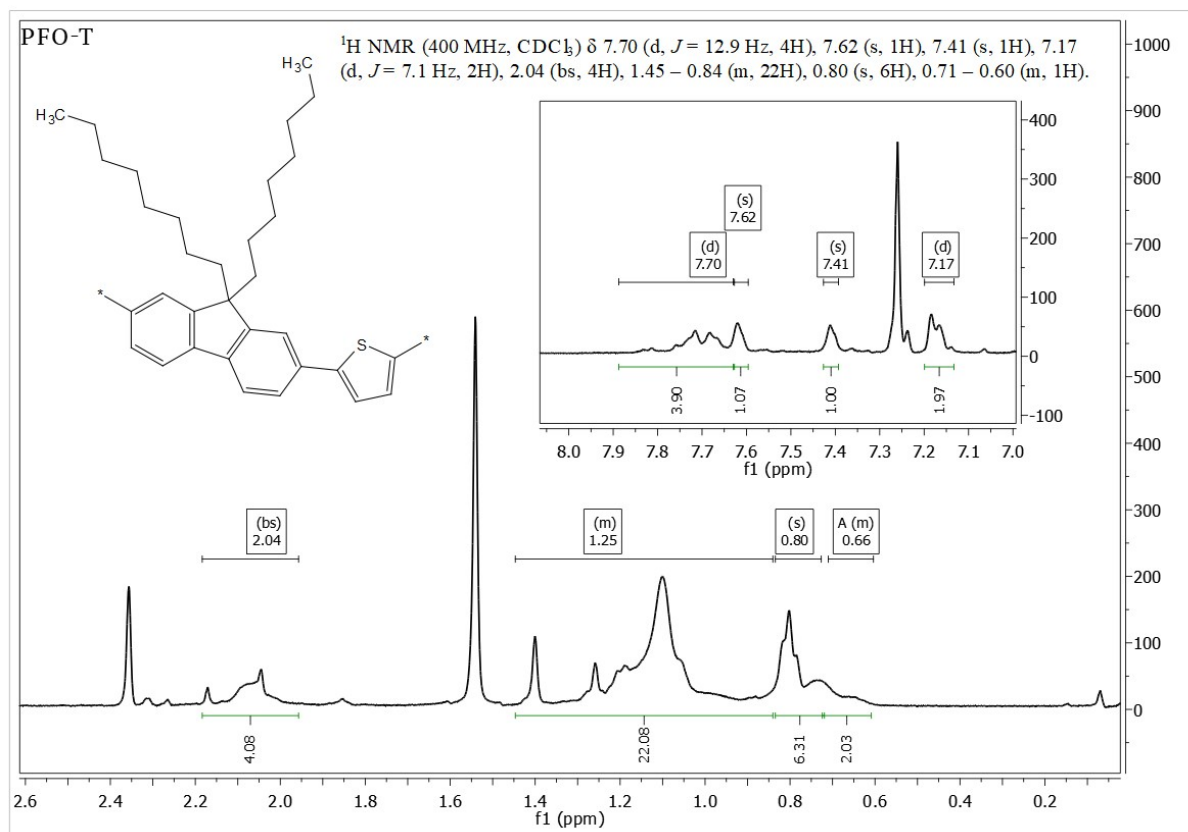
Figure S1 ^{1}H NMR spectrum of PFO-T synthesized in-house.
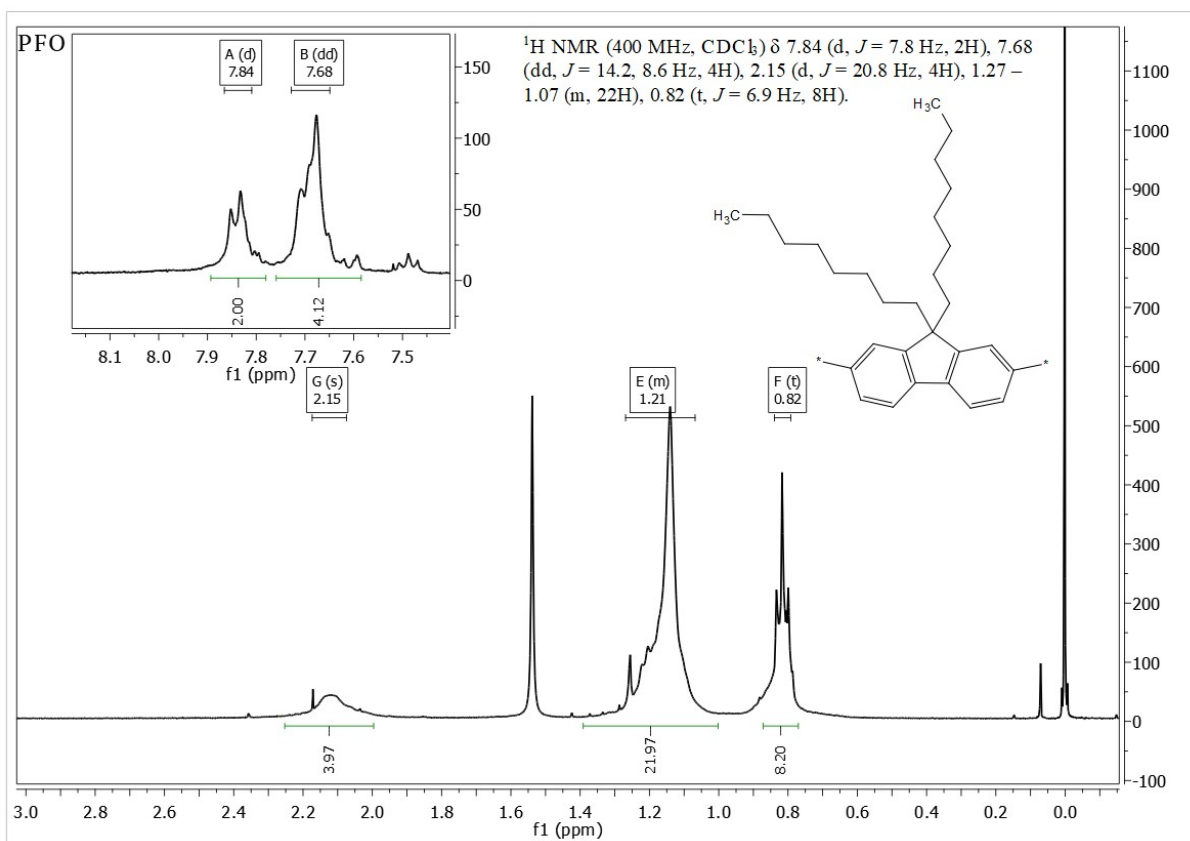
Figure S2 ^{1}H NMR spectrum of PFO synthesized in-house.
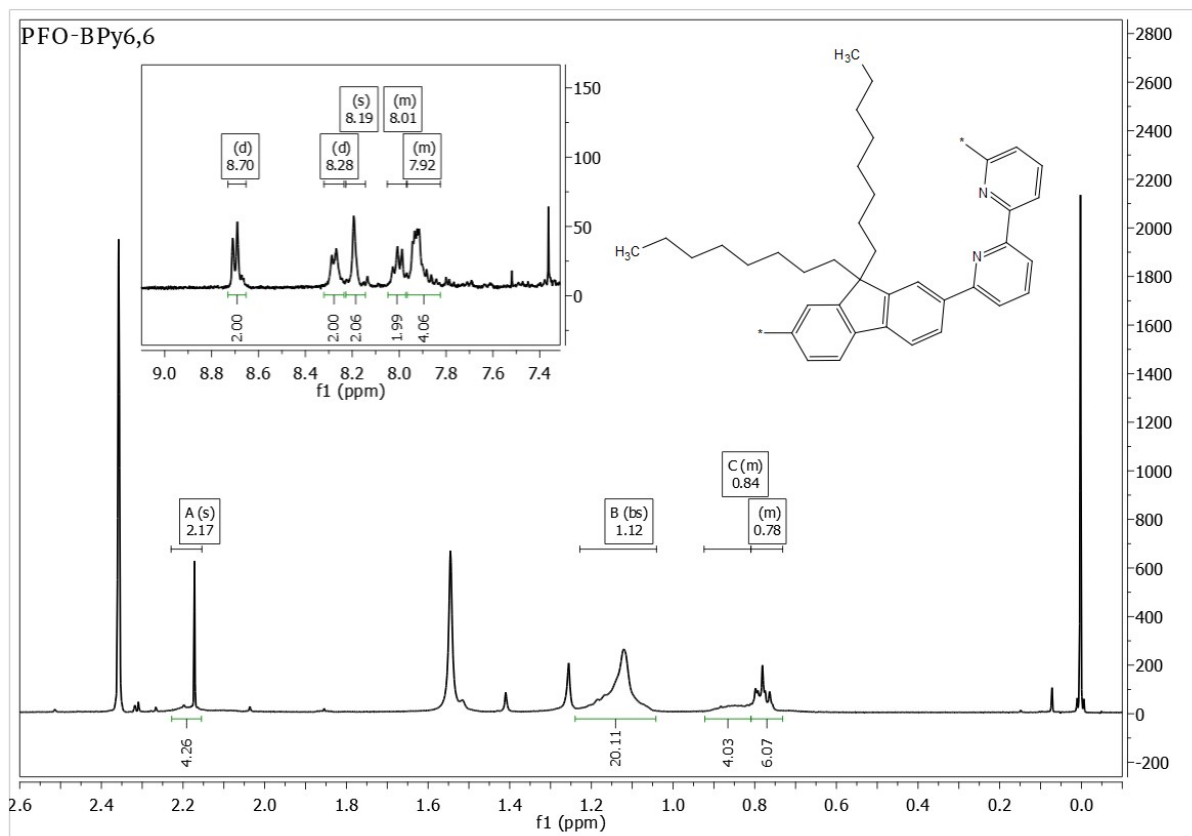
Figure S3 ^{1}H NMR spectrum of PFO-BPy6,6' synthesized in-house.

## 3.2. Size Exclusion Chromatography (SEC)

Molecular characteristics of the synthesized polymers, i.e., molecular weights and dispersity (Đ) indices were measured using a Size Exclusion Chromatograph (SEC, 1100 Agilent 1260 Infinity) (Agilent Technologies). The setup was equipped with an isocratic pump, autosampler, degasser, a thermostatic box for columns, and a differential refractometer MDS RI Detector. For data acquisition and processing, Addon Rev. B.01.02 data analysis software (Agilent Technologies) was employed. Linear polystyrene standards (580–300,000 g/mol) were used for the calibration, enabling the determination of SEC-calculated molecular weight. A pre-column guard (5 μm, 50 × 7.5 mm) and two columns (PLGel 5 μm MIXED-C 300 × 7.5 mm and PLGel 5 μm MIXED-D 300 × 7.5 mm), were used for the separation of the analytes. The measurements were conducted using $CHCl_3$ (HPLC grade) as the solvent (flow rate of the solvent: 0.8 mL/min, room temperature: 30 °C).

3.3. Absorption spectroscopy

Optical absorption spectra of freshly collected supernatants were measured within the wavelength range of 280–1100 nm using a Hitachi U-2910 spectrophotometer and a wider range of 300–1600 nm using a PerkinElmer Lambda 1050 spectrophotometer. A double beam mode was used with a pure solvent cuvette placed in the reference channel. Measurement was performed using 5 mm quartz cuvettes.

3.4. Deconvolution of absorption spectra

Deconvolution was performed using the Voigt function with the PTF Fit application [28]. Due to large redshifts between the observed peak positions in organic solvents and the values determined by Weisman in D_2O [29], it was necessary to tune the reference file to enable accurate peak fitting. The generated spectral data for a broad range of SWCNT types was used for further analysis. An example of the absorbance spectrum deconvoluted using this approach is shown below.
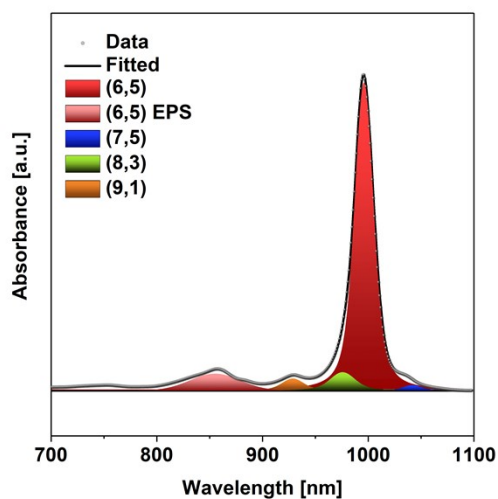
Figure S4 Deconvolution of the optical absorbance spectrum of (6,5)-enriched CoMoCAT SWCNTs suspended with PFO-BPy (EPS – electron-phonon sideband).
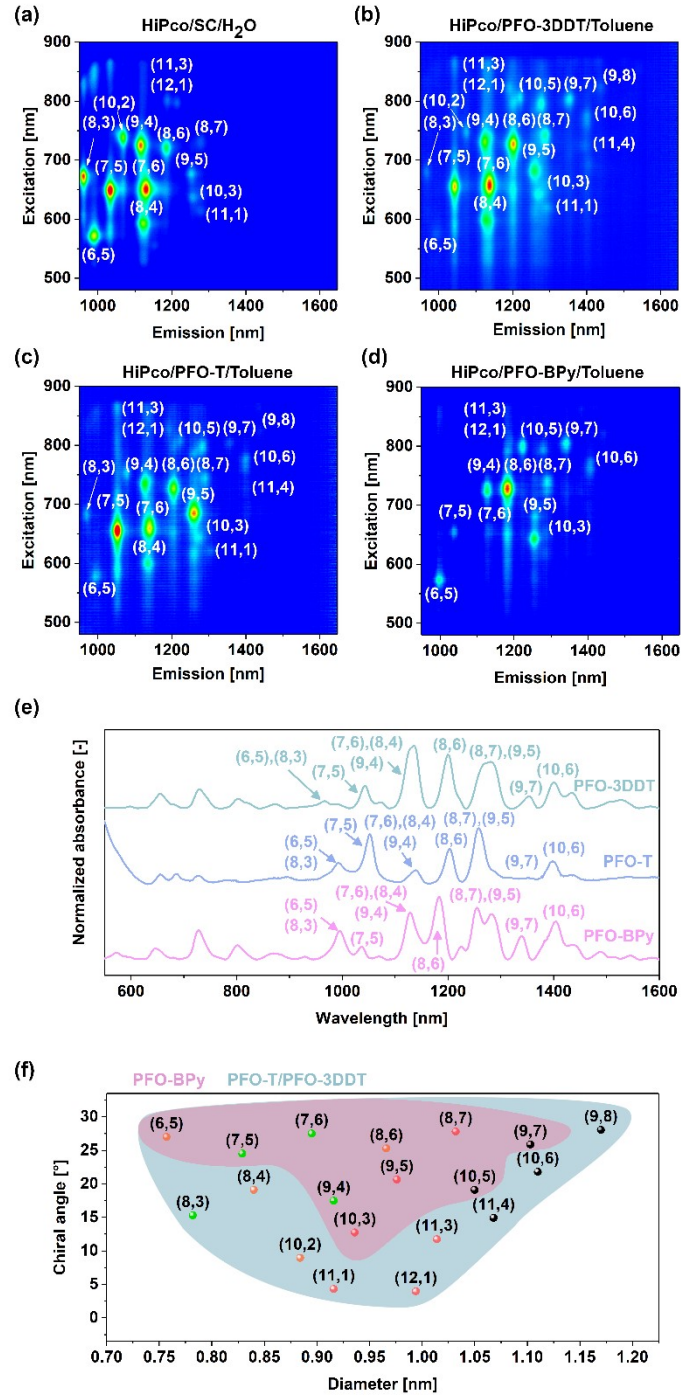
3.5. PL excitation-emission mapping

Excitation-emission photoluminescent maps (PL) were acquired using a ClaIR microplate reader (Photonetc, Canada). The data were registered in the ranges of 480–900 nm (excitation) and 900–1600 nm (emission). The results were then visualized using OriginPro 2022 software.

4. Results
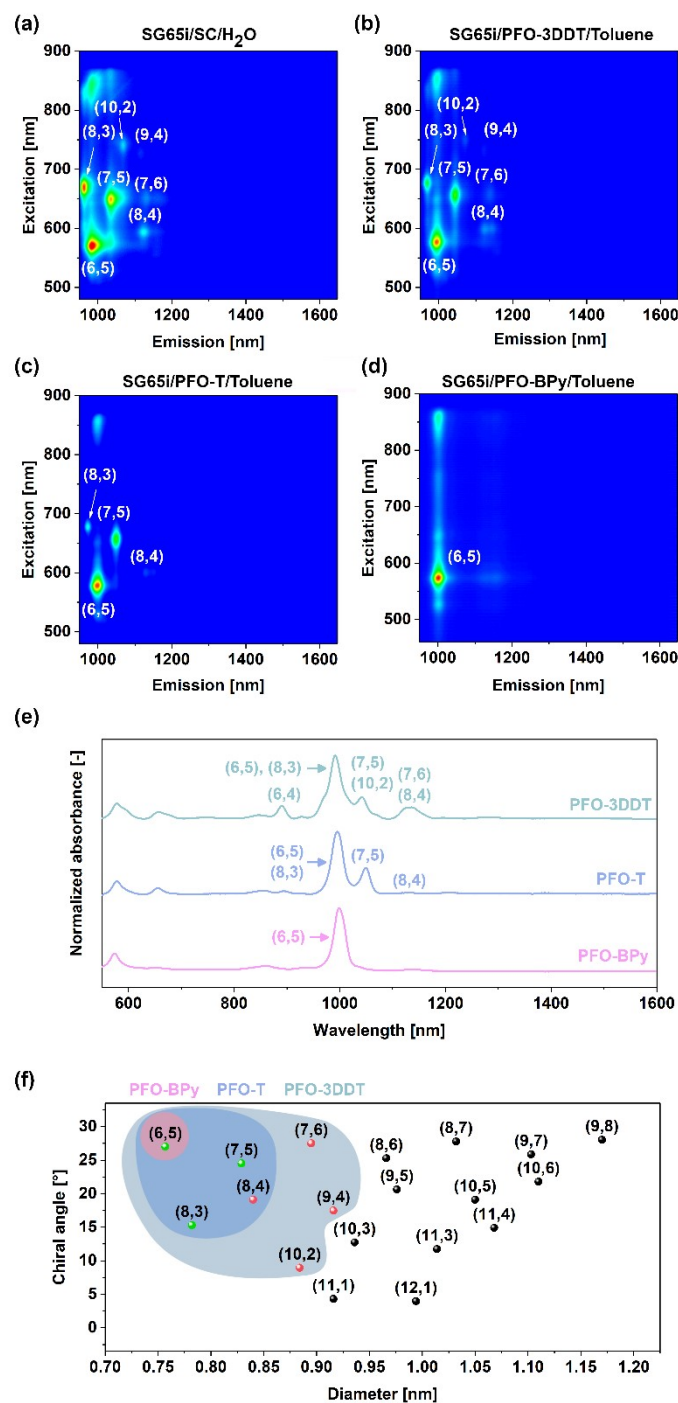
Figure S5 PL excitation-emission maps of (6,5)-enriched CoMoCAT SWCNTs suspended with (a) SC/H$_2$O, (b) PFO-3DDT/toluene, (c) PFO-T/toluene, and (d) PFO-BPy/toluene. (e) Optical absorbance spectra of SWCNT supernatants generated in toluene using the specified polymers. (f) Affinity of the evaluated polymers toward particular SWCNTs (green and red markers indicate abundant and scarce SWCNT types, respectively, determined based on the PL map of SC-based H$_2$O suspension of SWCNTs having indiscriminate solubilizing capabilities).

Figure S6 PL excitation-emission maps of HiPco SWCNTs suspended with (a) SC/H$_2$O, (b) PFO-3DDT/toluene, (c) PFO-T/toluene, and (d) PFO-BPy/toluene. (e) Optical absorbance spectra of SWCNT supernatants generated in toluene using the specified polymers. (f) The affinity of the evaluated polymers toward particular SWCNTs (green, orange, and red market indicate abundant, present, and scarce SWCNT types, respectively, determined based on the PL map of SC-based H$_2$O suspension of SWCNTs having indiscriminate solubilizing capabilities).

14

Table S2 Molecular characteristics of the synthesized polymer batches measured by GPC.

Polymer Name	Abbreviation	Mn [kg/mol]	Mw [kg/mol]	Đ
Poly(9,9'-dioctylfluorenyl-2,7-diyl-*alt*-6,6'-(2,2'-bipyridine))	PFO-BPy 6,6' (P1)	3900	6640	1.7
Poly(9,9'-dioctylfluorenyl-2,7-diyl-*alt*-5,5'-(2,2'-bipyridine))	PFO-BPy 5,5' (P2)	1780	4640	2.61
Poly(9,9'-dioctylfluorenyl-2,7-diyl-alt-5,5'-(2,2'-bipyridine))	PFO-BPy 5,5' (P3)	2840	3420	1.2
Poly(9,9'-dioctylfluorenyl-2,7-diyl)	PFO (P4)	15610	49741	3.19
Poly(9,9'-dioctylfluorenyl-2,7-diyl-*alt*-2,5-tiophene)	PFO-T (P5)	3250	4230	1.3
Poly(9,9'-dioctylfluorenyl-2,7-diyl-*alt*-2,5-tiophene)	PFO-T (P6)	3020	4880	1.62
Poly(9,9'-dioctylfluorenyl-2,7-diyl-*alt*-2,5-tiophene)	PFO-T (7)	5190	6800	1.31
Poly(9,9'-dioctylfluorenyl-2,7-diyl-*alt*-2,5-tiophene)	PFO-T (P8)	4880	7370	1.51
Poly(9,9'-dioctylfluorenyl-2,7-diyl-*alt*-2,5-tiophene)	PFO-T (P9)	5620	8000	1.42
Poly(9,9'-dioctylfluorenyl-2,7-diyl-*alt*-2,5-tiophene)	PFO-T (10)	5550	8550	1.54
Poly(9,9'-dioctylfluorenyl-2,7-diyl-*alt*-2,5-tiophene)	PFO-T (P11)	8200	25900	3.16
Poly(9,9'-dioctylfluorenyl-2,7-diyl-*alt*-2,5-(3-dodecyltiophene))	PFO-3DDT (P12)	17800	42150	2.37
Poly(9-(9-heptadecyl)-carbazoly-2,7-diyl-*alt*-6,6'-(2,2'-bipirydyl))	PCz-BPy6,6 (P13)	27800	78300	2.82
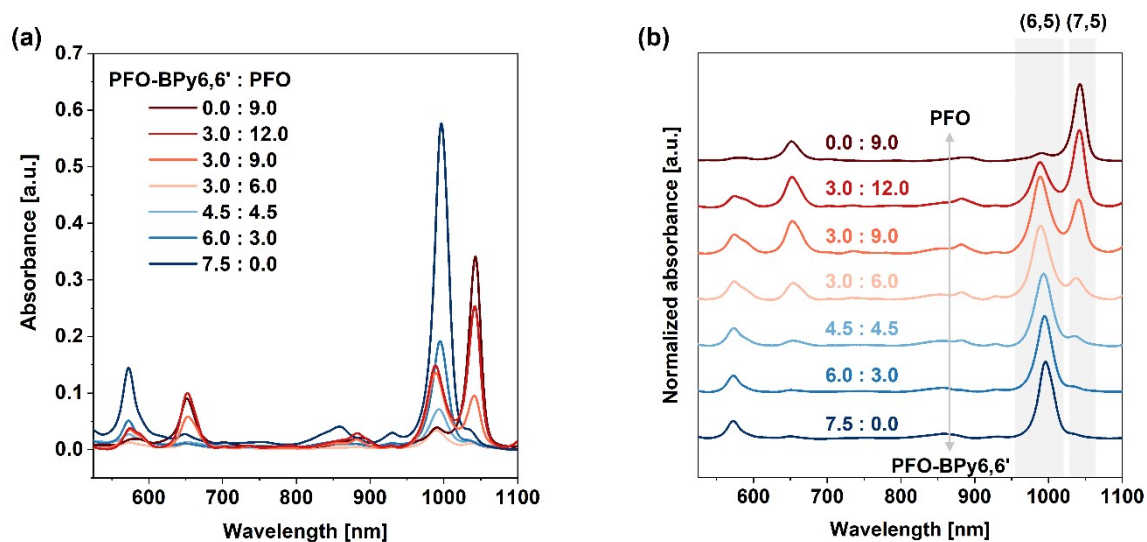
Figure S7 The influence of PFO:PFO-BPy6,6' ratio (in milligrams per 1.5 mg raw (6,5)-enriched CoMoCAT SWCNTs and 8 mL of toluene) on the (a) yield and (b) selectivity of extraction. Molecular characteristics of the employed polymers were as follows: PFO M_n=15,610 kg/mol, M_w=49 741 kg/mol, Đ=3.19 and PFO-BPy6,6' M_n=3,904 kg/mol, M_w=6,637 kg/mol, Đ=1.7.
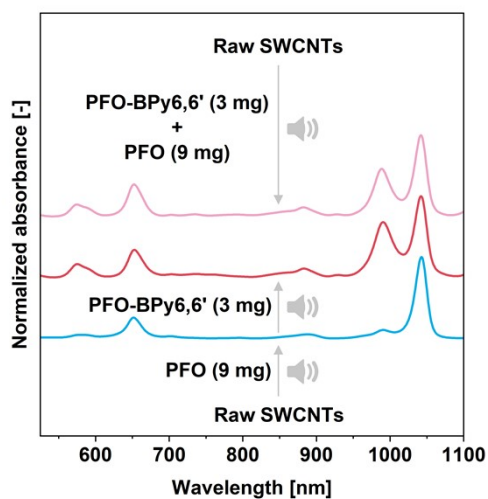
**Figure S8** Double sonication technique (first SWCNTs were homogenized in the presence of PFO, then PFO-BPy6,6' was added to the as-generated suspension, and the mixture was once again processed by sonication), showing that a conjugated polymer of higher binding strength (PFO-BPy6,6') may replace another one exhibiting weaker interaction with the SWCNT surface (PFO). (6,5)-enriched CoMoCAT SWCNTs were processed.
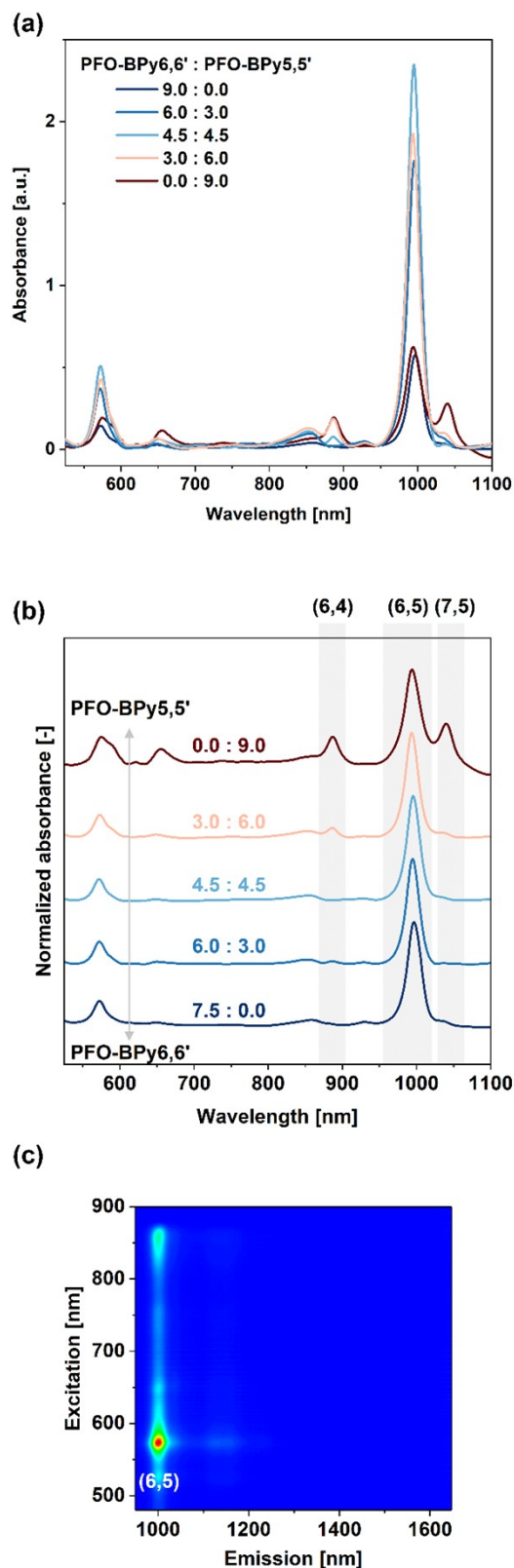
Figure S9 The influence of PFO-BPy5,5':PFO-BPy6,6' ratio (in milligrams per 1.5 mg raw (6,5)-enriched CoMoCAT SWCNTs and 8 mL of toluene) on the (a) yield and (b) selectivity of extraction. (c) PL excitation-emission map confirming the high purity of the obtained material (4:5/4:5 mg/mg ratio). (6,5)-enriched CoMoCAT SWCNTs were processed.
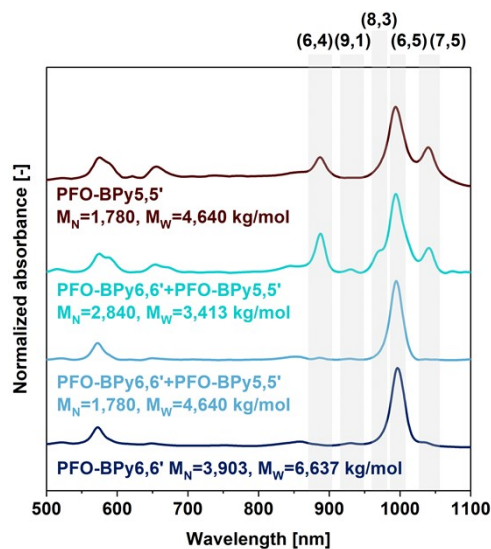
Figure S10 The influence of molecular characteristics of PFO-BPy5,5' on the quality of the obtained SWCNT suspension from (6,5)-enriched CoMoCAT SWCNTs gauged using absorbance spectroscopy.
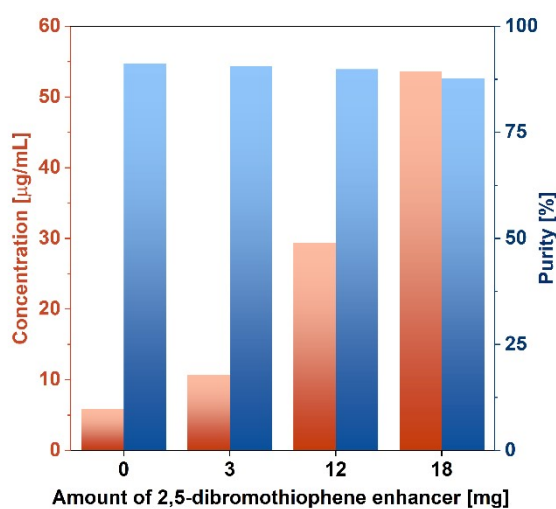

Figure S11 Purity and concentration of the extracted (6,5) SWCNT species as a function of the amount of introduced 2,5-dibromothiophene enhancer (per 1.5 mg of raw SWCNTs and 6 mg of PFO-BPy6,6'). Recorded optical absorption spectra of SWCNT suspensions were deconvoluted according to the procedure described above to carry out the quantification.

To exclude the possibility that the comparison of the molecular enhancers presented in Figure 2b was affected by the molecular weight of these compounds, equimolar amounts of these compounds were added, and the optical absorbance spectra were measured upon SWCNT sonication and centrifugation (Figure S11). Even after the exclusion of this factor, 2,5-dibromothiophene still could be classified as the strongest extraction promoter.

Table S3. Calculation of the amount of CPE enhancer needed to introduce the same number of moles as 2,5-dibromothiophene, which showed the highest performance.

Compound name	M [g/mol]	m [mg] equivalent to 0.0744 mmol of 2,5-dibromothiophene
6,6'-Dibromo-2,2'-bipyridine	313.98	23.36
5,5'-Dibromo-2,2'-bipyridine	313.98	23.36
2,5-dibromo-3-dodecylthiophene	410.25	30.52
2,5-dibromo-3-hexylthiophene	326.09	24.26
2,5-dibromothiophene	241.93	18.00
thiophene	84.14	6.26
2,7-dibromo-9,9-dioctylfluorene	548.44	40.80
9,9-di-n-octylfluorene-2,7-diboronic acid bis(pinacol)ester	642.57	47.81
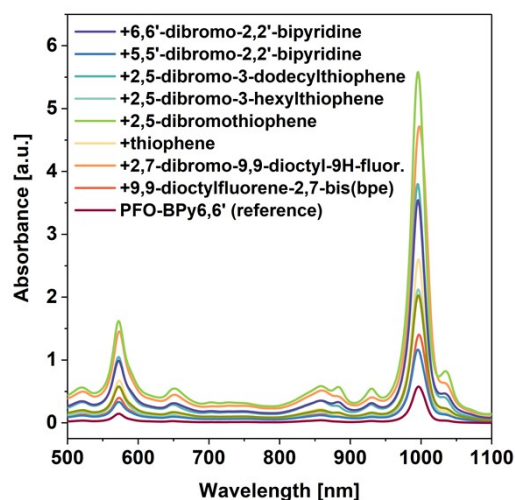
Figure S12 The effect of the addition of 0.0744 mmol of various molecular enhancers (equivalent to 18 mg of 2,5-dibromothiophene) compared with sole use of PFO-BPy6,6' polymer to purify (6,5)-enriched CoMoCAT SWCNTs.

The results presented in Figure S13(b) show that only for the highest concentration of 2,5-dibromothiophene molecules in the solution (30 molecules, 8:3 enhancer:polymer weight ratio), the probability of finding the polymer next to SWCNT was higher than in the absence of 2,5-dibromothiophene molecules (cf. the intensities of first and second peaks of CNT-polymer RDFs). Detailed analysis showed that two distinct parts of the polymer, its backbone, and its side chains, behaved differently. As shown in Figure S13(c), it was more likely to find the polymer backbone next to the SWCNT when not only 30 but also 20 molecules of 2,5-dibromothiophene were added to the solution. But only after the addition of 30 molecules of 2,5-dibromothiophene, the probability of finding the polymer side chains next to SWCNT increased above the level for the system without any 2,5-dibromothiophene molecules.

The intensities of all peaks in C_{ring}-CNT and C_{chain}-CNT RDFs after the addition of 10 2,5-dibromothiophene molecules were significantly smaller with respect to the system without any enhancer molecules. However, for 10 enhancer molecules present in the solution, the RDF peaks, especially the second peaks, were much broader. This information, together with analysis of the mass density profile for this case (Figure 3c, second graph from the left), suggested that this was due to a few polymer units being moved from the initial almost parallel position along SWCNT to the start wrapping around CNT surface (Fig. 3a). Effectively part of the polymer was positioned perpendicularly to the CNT axis making only one polymer unit in its backbone close to the SWCNT lateral surface, leaving two units further away. Because of the length of the modeled polymer (only 5 repeatable units), it had a significant impact on the RDF plot. Importantly, the simulations were relatively short, and it was expected that over a longer timescale, due to the enhanced interactions between nanotube and polymer induced by the presence of 2,5-dibromothiophene molecules in the solution, the effective wrapping of the polymer around SWCNT would be tighter than without the addition of any enhancer molecules.
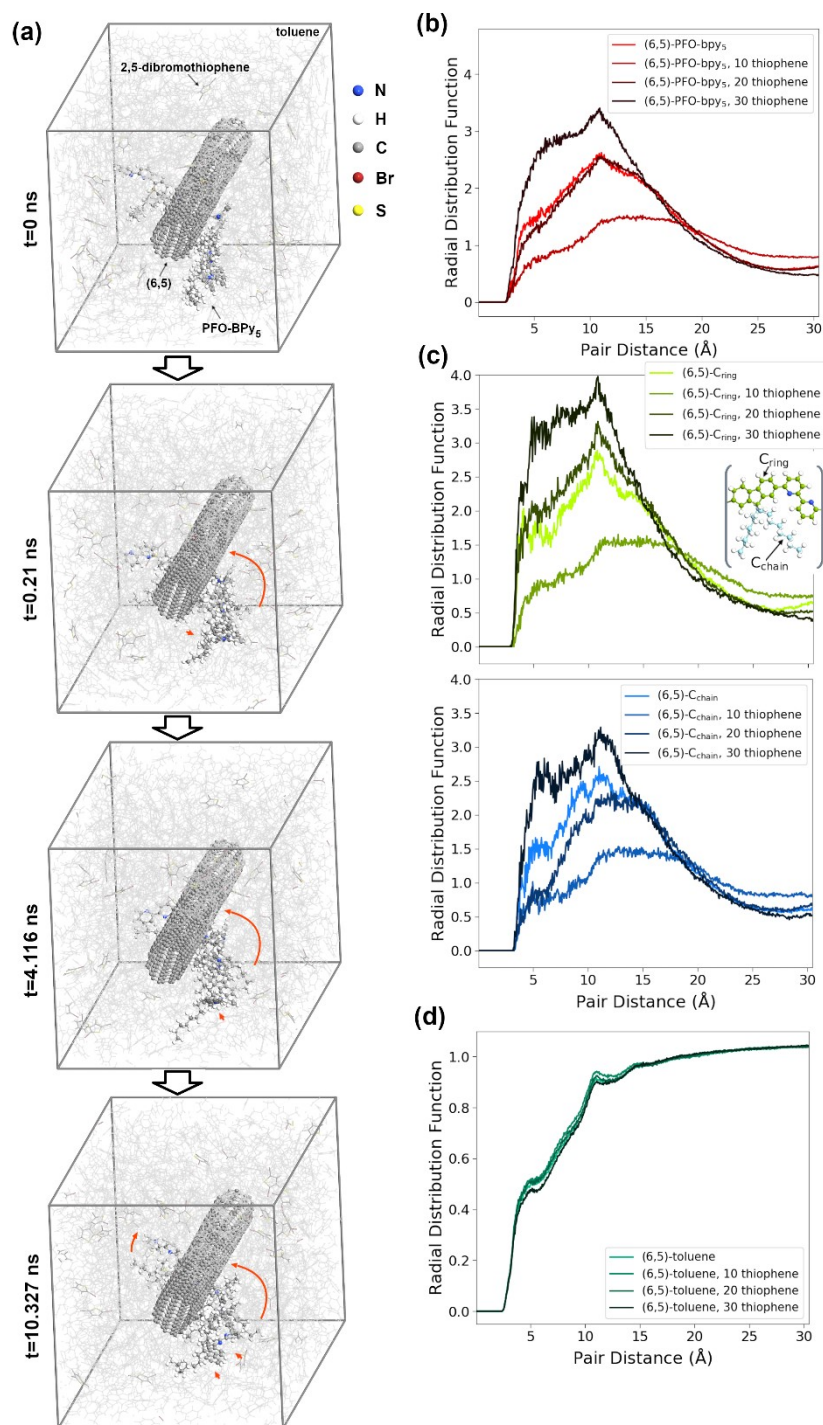
Figure S13 (a) The polymer wrapping stages. Snapshots from MD/MC simulations of two units of (6,5) SWCNT interacting with PFO-BPy6,6' polymer (five repeatable units) in the presence of 30 2,5-dibromothiophene molecules immersed in toluene (1000 molecules) solution. (b) Radial distribution functions (RDFs) of nanotube-polymer atoms for systems containing 0, 10, 20, or 30 2,5-dibromothiophene molecules. The probability of finding polymer next SWCNT was the highest for systems containing 30 2,5-dibromothiophene molecules. (c) RDFs between nanotube carbon and polymer backbone carbon (C_{ring}) atoms, nanotube carbon, and polymer side chain (C_{chain}) atoms. Inset: A schematic diagram showing two distinct regions of PFO-BPy6,6' polymer: the backbone and the side chains. (d) RDFs between nanotube and toluene for all considered systems. 30 molecules of 2,5-dibromothiophene molecules also impacted the interactions between the nanotube and the solvent making finding the solvent molecules in the direct vicinity of the nanotube less probable.
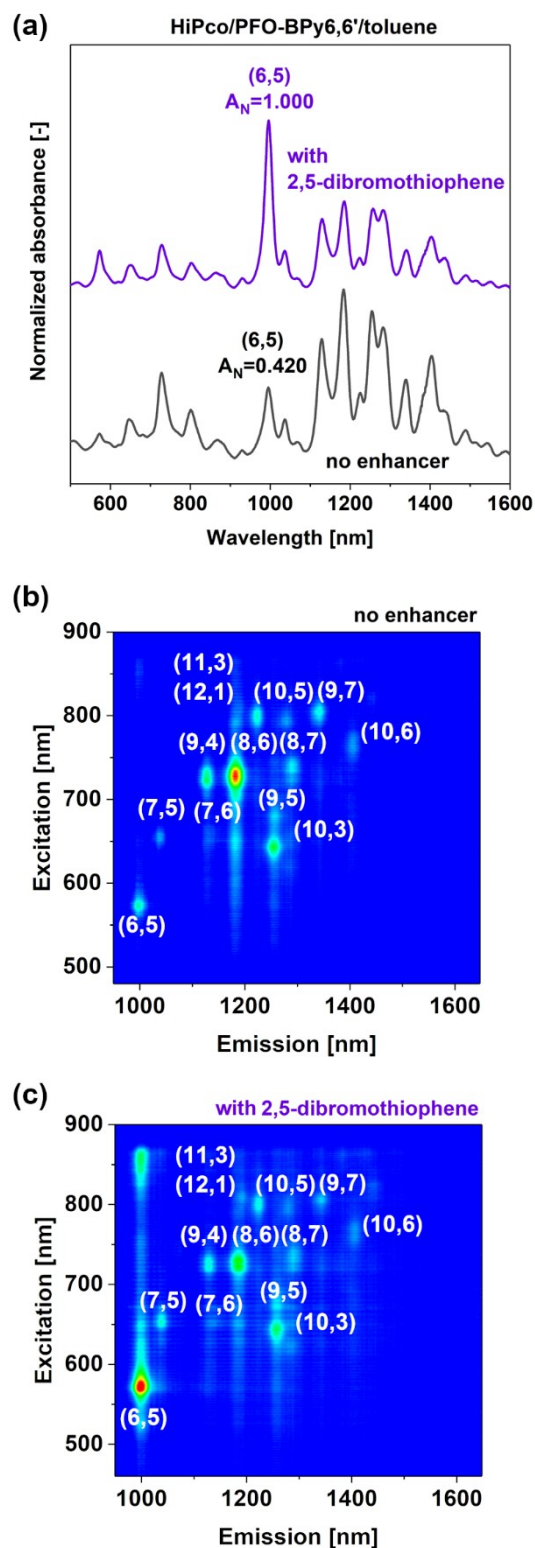
Figure S14 (a) The impact of the use of 2,5-dibromothiophene CPE enhancer on the composition of the material extracted from HiPco SWCNTs. A_N stands for normalized absorbance, i.e., the ratio of intensity of the (6,5) SWCNT peak to the intensity of the highest peak in the spectrum, (b,c) corresponding PL excitation-emission maps.

Without the enhancer, (8,6) SWCNTs of Θ=25.29° dominated the suspension, while the addition of the enhancer made the suspension rich in (6,5) SWCNTs Θ=27.00°. It is evident that the polymer preferred specific chiral angles. Still, the addition of the enhancer favored the wrapping of SWCNTs of smaller diameter type: d(6,5)=0.757 nm vs. d(8,6)=9.658 nm. Firstly, the results support a theory postulated in this article that the small molecular chaperones facilitate the encapsulation of SWCNTs with the polymer chains without affecting the selectivity of the polymer. Secondly, interestingly, the presence of the enhancer molecules promotes individualization of smaller, much less abundant species, such as (6,5) SWCNTs, the bundles of which are usually harder to break and disperse in a liquid medium, compared to agglomerates of larger SWCNTs. Simultaneously, the results show that the effectiveness of the CPE approach hinges on the composition of the raw SWCNT material. The SWCNT mixture should ideally contain only a single SWCNT type with a chiral angle preferred by the conjugated polymer employed for sorting.

5. References

(1) Neyts, E. C.; Bogaerts, A. Combining Molecular Dynamics with Monte Carlo Simulations: Implementations and Applications. *Theor Chem Acc* **2013**, 132 (2), 1–12. https://doi.org/10.1007/s00214-012-1320-x.

(2) Bal, K. M.; Neyts, E. C. On the Time Scale Associated with Monte Carlo Simulations. *J Chem Phys* **2014**, 141 (20), 204104. https://doi.org/10.1063/1.4902136.

(3) Martinez, L.; Andrade, R.; Birgin, E. G.; Martínez, J. M. PACKMOL: A Package for Building Initial Configurations for Molecular Dynamics Simulations. *J Comput Chem* **2009**, 30 (13), 2157–2164. https://doi.org/10.1002/jcc.21224.

(4) Bitzek, E.; Koskinen, P.; Gähler, F.; Moseler, M.; Gumbsch, P. Structural Relaxation Made Simple. *Phys Rev Lett* **2006**, 97 (17), 170201. https://doi.org/10.1103/PhysRevLett.97.170201.

(5) Berendsen, H. J. C.; Postma, J. P. M.; van Gunsteren, W. F.; DiNola, A.; Haak, J. R. Molecular Dynamics with Coupling to an External Bath. *J Chem Phys* **1984**, 81 (8), 3684–3690. https://doi.org/10.1063/1.448118.

(6) Martyna, G. J.; Klein, M. L.; Tuckerman, M. Nosé–Hoover Chains: The Canonical Ensemble via Continuous Dynamics. *J Chem Phys* **1992**, 97 (4), 2635–2643. https://doi.org/10.1063/1.463940.

(7) Liu, D. C.; Nocedal, J. On the Limited Memory BFGS Method for Large Scale Optimization. *Math Program* **1989**, 45 (1), 503–528. https://doi.org/10.1007/BF01589116.

(8) K. Rappe, A.; J. Casewit, C.; S. Colwell, K.; A. Goddard III, W.; M. Skiff, W. UFF, a Full Periodic Table Force Field for Molecular Mechanics and Molecular Dynamics Simulations. *J Am Chem Soc* **2002**, 114 (25), 10024–10035. https://doi.org/10.1021/ja00051a040.

(9) Schneider, J.; Hamaekers, J.; Chill, S. T.; Smidstrup, S.; Bulin, J.; Thesen, R.; Blom, A.; Stokbro, K. ATK-ForceField: A New Generation Molecular Dynamics Software Package. *Model Simul Mat Sci Eng* **2017**, 25 (8), 085007. https://doi.org/10.1088/1361-651X/aa8ff0.

(10) *https://www.synopsys.com/silicon/quantumatk.html.*

(11) Essmann, U.; Perera, L.; Berkowitz, M. L.; Darden, T.; Lee, H.; Pedersen, L. G. A Smooth Particle Mesh Ewald Method. *J Chem Phys* **1995**, 103 (19), 8577–8593. https://doi.org/10.1063/1.470117.

(12) K. Rappe, A.; A. Goddard III, W. Charge Equilibration for Molecular Dynamics Simulations. *J Phys Chem* **2002**, 95 (8), 3358–3363. https://doi.org/10.1021/j100161a070.

(13) Lennard-Jones, J. E. Cohesion. *Proceedings of the Physical Society* **1931**, 43 (5), 461–482. https://doi.org/10.1088/0959-5309/43/5/301.

(14) Jones, J. E.; Chapman, S. On the Determination of Molecular Fields. —II. From the Equation of State of a Gas. *Proceedings of the Royal Society of London*. Series A, Containing Papers of a Mathematical and Physical Character **1997**, 106 (738), 463–477. https://doi.org/10.1098/rspa.1924.0082.

(15) Jones, J. E.; Chapman, S. On the Determination of Molecular Fields.—I. From the Variation of the Viscosity of a Gas with Temperature. *Proceedings of the Royal Society of London*. Series A, Containing Papers of a Mathematical and Physical Character **1997**, 106 (738), 441–462. https://doi.org/10.1098/rspa.1924.0081.

(16) Kohn, W.; Sham, L. J. Self-Consistent Equations Including Exchange and Correlation Effects. *Physical Review* **1965**, 140 (4A), A1133–A1138. https://doi.org/10.1103/PhysRev.140.A1133.

(17) Hohenberg, P.; Kohn, W. Inhomogeneous Electron Gas. *Physical Review* **1964**, 136 (3B), B864–B871. https://doi.org/10.1103/PhysRev.136.B864.

(18) Wilk A N, L.; Nusair, D. M. Accurate Spin-Dependent Electron Liquid Correlation Energies for Local Spin Density Calculations: A Critical Analysis1; **1980**; Vol. 58.

(19) J. Stephens, P.; J. Devlin, F.; F. Chabalowski, C.; J. Frisch, M. Ab Initio Calculation of Vibrational Absorption and Circular Dichroism Spectra Using Density Functional Force Fields. J Phys Chem **2002**, 98 (45), 11623–11627. https://doi.org/10.1021/j100096a001.

(20) Lee, C.; Yang, W.; Parr, R. G. Development of the Colle-Salvetti Correlation-Energy Formula into a Functional of the Electron Density. *Phys Rev B* **1988**, 37 (2), 785–789. https://doi.org/10.1103/PhysRevB.37.785.

(21) Becke, A. D. Density-functional Thermochemistry. III. The Role of Exact Exchange. *J Chem Phys* **1993**, 98 (7), 5648–5652. https://doi.org/10.1063/1.464913.

(22) Smidstrup, S.; Markussen, T.; Vancraeyveld, P.; Wellendorff, J.; Schneider, J.; Gunst, T.; Verstichel, B.; Stradi, D.; Khomyakov, P. A.; Vej-Hansen, U. G.; Lee, M.-E.; Chill, S. T.; Rasmussen, F.; Penazzi, G.; Corsetti, F.; Ojanperä, A.; Jensen, K.; Palsgaard, M. L. N.; Martinez, U.; Blom, A.; Brandbyge, M.; Stokbro, K. QuantumATK: An Integrated Platform of Electronic and Atomic-Scale Modelling Tools. *Journal of Physics: Condensed Matter* **2020**, 32 (1), 015901. https://doi.org/10.1088/1361-648X/ab4007.

(23) Wykes, M.; Milián-Medina, B.; Gierschner, J. Computational Engineering of Low Bandgap Copolymers. *Front Chem* **2013**, 1.

(24) Elhaes, H.; Morsy, M.; Yahia, I. S.; Ibrahim, M. Molecular Modeling Analyses for Electronic Properties of CNT/TiO2 Nanocomposites. *Opt Quantum Electron* **2021**, 53 (5), 269. https://doi.org/10.1007/s11082-021-02945-5.

(25) Chełmecka, E.; Pasterny, K.; Kupka, T.; Stobiński, L. DFT Studies of COOH Tip-Functionalized Zigzag and Armchair Single Wall Carbon Nanotubes. *J Mol Model* **2012**, 18 (5), 2241–2246. https://doi.org/10.1007/s00894-011-1242-x.

(26) Ye, G.; Talsma, W.; Tran, K.; Liu, Y.; Dijkstra, S.; Cao, J.; Chen, J.; Qu, J.; Song, J.; Antonietta Loi, M.; C. Chiechi, R. Polar Side Chains Enhance Selection of Semiconducting Single-Walled Carbon Nanotubes by Polymer Wrapping. *Macromolecules* **2022**, 55 (4), 1386–1397. https://doi.org/10.1021/acs.macromol.1c01842.

(27) Monkhorst, H. J.; Pack, J. D. Special Points for Brillouin-Zone Integrations. *Phys Rev B* **1976**, 13 (12), 5188–5192. https://doi.org/10.1103/PhysRevB.13.5188.

(28) Pfohl, M.; D. Tune, D.; Graf, A.; Zaumseil, J.; Krupke, R.; S. Flavel, B. Fitting Single-Walled Carbon Nanotube Optical Spectra. *ACS Omega* **2017**, 2 (3), 1163–1171. https://doi.org/10.1021/acsomega.6b00468.

(29) Weisman, R. B.; Bachilo, S. M. Dependence of Optical Transition Energies on Structure for Single-Walled Carbon Nanotubes in Aqueous Suspension: An Empirical Kataura Plot. *Nano Lett* **2003**, 3 (9), 1235–1238. https://doi.org/10.1021/nl034428i.